molecular pharmaceutics

Article

pubs.acs.org/molecularpharmaceutics

Grafting Aptamers onto Gold Nanostars Increases *in Vitro* Efficacy in a Wide Range of Cancer Cell Types

Duncan Hieu M. Dam,[†] Kayla S. B. Culver,[‡] and Teri W. Odom*[,†,‡]

[†]Department of Chemistry, Northwestern University, 2145 Sheridan Road, Evanston, Illinois 60208, United States

[‡]Department of Materials Science and Engineering, Northwestern University, 2145 Sheridan Road, Evanston, Illinois 60208, United States

Supporting Information

ABSTRACT: We report the design of a nanoconstruct that can function as a cell-type independent agent by targeting the ubiquitous protein nucleolin. Gold nanostars (AuNS) loaded with high densities of nucleolin-specific DNA aptamer AS1411 (Apt-AuNS) produced anticancer effects in a panel of 12 cancer lines containing four representative subcategories. We found that the nanoconstructs could be internalized by cancer cells and trafficked to perinuclear regions. Apt-AuNS resulted in downregulation of antiapoptotic Bcl-2 mRNA expression by ca. 200% compared to cells without the nanoconstructs. The caspase 3/7 activity (apoptosis) and cell death in cancer cells treated with Apt-AuNS increased by 1.5 times and by ca. 17%, respectively, compared to cells treated with free AS1411 at over 10 times the concentration. Moreover, light-triggered release of aptamer from the AuNS further enhanced the *in vitro* efficacy of the nanoconstructs in the cancer line panel with a 2-fold increase in caspase activity and a 40% decrease in cell viability compared to treatment with Apt-AuNS only. In contrast, treatments of the nanoconstructs with or without light-triggered release on a panel of normal cell lines had no adverse effects.

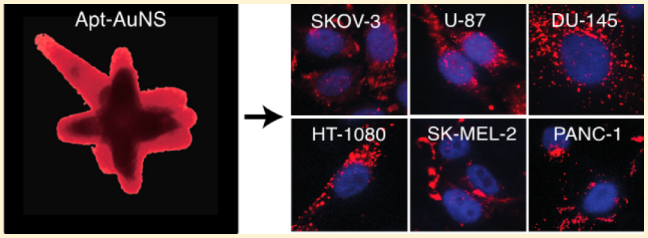

KEYWORDS: *aptamers, gold nanostars, nucleolin, anticancer agents*

INTRODUCTION

Targeted therapy relies on cell-surface receptors to direct anticancer agents to tumors.[1−3] Because of the selectivity to cancer cells, this type of treatment has shown improvements in patient quality of life by reducing unwanted side effects of nontargeted drugs, such as those utilized in chemotherapy.[4−6] However, cancer cell populations within the same tumor are often diverse and exhibit various cell-surface receptors; hence, different types of treatment are usually necessary to eradicate all of the cancer cells.[6,7] Recurrence rates of cancers after targeted treatment can be as high as 50%[8] because of the regeneration of cancer cells that cannot be eliminated.[9] One solution to overcome this problem is to target a cell-surface receptor that is ubiquitous. Nucleolin has recently been investigated as a surface receptor that can also transport targeting molecules from the plasma membrane to the nucleus of cancer cells.[10,11] The overexpression of nucleolin on the cell surface and in the cytoplasm of exponentially growing cells suggests that this protein, whose one of the primary roles is to shuttle molecules between the nucleus and the cytoplasm, can function as a receptor for cell-type independent targeted cancer treatment.[11−14]

Monoclonal antibodies (mAbs) are the key anticancer agents employed in targeted therapy; however, off-target effects and immunogenic responses can result in severe side effects.[15] One emerging alternative to mAbs is aptamers, synthetic oligonucleotides that can fold and bind to specific moieties on targeted molecules.[16,17] The DNA aptamer AS1411 (26-mer, 7.8 kDa) has shown high binding affinity to nucleolin (K_d is in pM to low nM range)[10] via its G-quadruplex structure. One important function of nucleolin is binding to the AU-rich components in the 3′-untranslated region of the antiapoptotic gene Bcl-2 mRNA as protection against mRNA degradation.[18,19] Free AS1411 can bind to nucleolin in the same area where nucleolin stabilizes Bcl-2 mRNA; hence, destabilization and subsequent down-regulation of Bcl-2 by AS1411 can result in apoptosis.[20] AS1411 has been tested in clinical trials for leukemia[21] and renal cell cancer;[22] however, there are some concerns based of fast clearance and premature degradation (half-life ∼5 h).[16,20,23−25]

To improve the stability of AS1411, we recently reported a strategy to attach AS1411 (Apt denotes the homodimer form) to the surface of gold nanostars (AuNS).[26] We found that high loading densities of Apt on the AuNS increased the overall stability of aptamers in physiological environments, similar to other reports of nucleic acids on spherical gold particles.[27] We evaluated aptamer-loaded AuNS (Apt-AuNS) in HeLa (cervical) cancer cells as a model system and were able to observe effects from the nanoconstruct interacting with the cell

Received: September 21, 2013
Revised: December 9, 2013
Accepted: January 14, 2014
Published: January 14, 2014

nucleus.[26] Apt-AuNS was trafficked by nucleolin from the cell surface to the perinuclear regions and induced folding of the nuclear envelope.[26] We demonstrated that these changes in nuclear phenotype could be directly correlated with disruption of cellular function, including increased double-stranded DNA breaks in the nucleus as well as escalation of caspase 3/7 activity and cell death.[26] The potential of Apt-AuNS as a general anticancer agent, however, has not been tested.

Here, we report that Apt-AuNS can function as a nanoconstruct resulting in *in vitro* efficacies superior to that of free aptamer biomolecules in a wide range of cancer cells. This study is the first to show that G-quadruplex aptamer homodimer-loaded nanoparticles can be effective in four major cancer subcategories. We found that nucleolin was abundant in plasma membrane and cytoplasm extracts of a 12-cancer cell panel. Expression of surface nucleolin was also higher in cancer cells compared to normal cells. Incubation of the cancer-cell panel with Apt-AuNS resulted in cellular uptake that was quantified by inductively coupled plasma-mass spectrometry (ICP-MS). The reformulation of AS1411 by grafting to AuNS enhanced the anticancer effects in all cancer cell lines with a 17% higher average cell death compared to free AS1411 exceeding 10 times the concentration. We also discovered that downregulation of Bcl-2 mRNA expression was a contributing factor to apoptosis. Furthermore, the *in vitro* efficacy of Apt-AuNS was improved by detaching aptamers from the AuNS nanocarrier inside cancer cells. Using ultrafast laser light to trigger the release of Apt, we showed that the average percentage of cell death increased to 65%, which is 55% higher compared to that of free AS1411 at over 10 times the concentration.

RESULTS AND DISCUSSION

Ubiquitous Expression of Nucleolin in Plasma Membrane and Cytoplasm of Cancer Cells. Because overexpression of nucleolin in the plasma membrane and cytoplasm is crucial for cellular uptake and trafficking of AS1411,[13,14] we first determined the non-nuclear nucleolin (cytoplasmic and plasma membrane) levels in a 12-cancer line panel using immunoblotting (Supporting Information, Materials and Methods). The cancer panel consisted of four types of subcategories: carcinoma, sarcoma, melanoma, and glioblastoma. We also included a control panel with three lines: HS-27 (skin fibroblast), WI-38 (lung fibroblast), and MCF-10A (epithelial mammary cell). We observed that the levels of full-length nucleolin (106 kDa) and its proteolysis product (98 kDa) in fibroblast-like cancer cells (HT-1080, fibrosarcoma and SK-MEL-2, melanoma) were up to four times higher compared to normal fibroblast cells (HS-27 and WI-38) (Figure 1). Regarding epithelial cells, the expression of nucleolin in cancer cells was 10 times higher on average than that of MCF-10A cells (Figure 1). The relative amounts of nucleolin were normalized to the expression of the housekeeping protein, *β*-actin. Although minimal expression of nucleolin was found in MCF-10A, high nucleolin levels in the non-nuclear extracts of HS-27 and WI-38 fibroblasts were seen (Figure 1B). This observation suggests that a normal cell panel containing both fibroblast and epithelial cells is necessary to assess effects of Apt-AuNS on different types of tissues.

Synthesis and Characterization of Aptamer-Loaded Gold Nanoconstructs. Apt-AuNS is a biocompatible nanoconstruct that has demonstrated excellent *in vitro* efficacy in HeLa cells.[26] The AuNS carrier was synthesized by reducing a

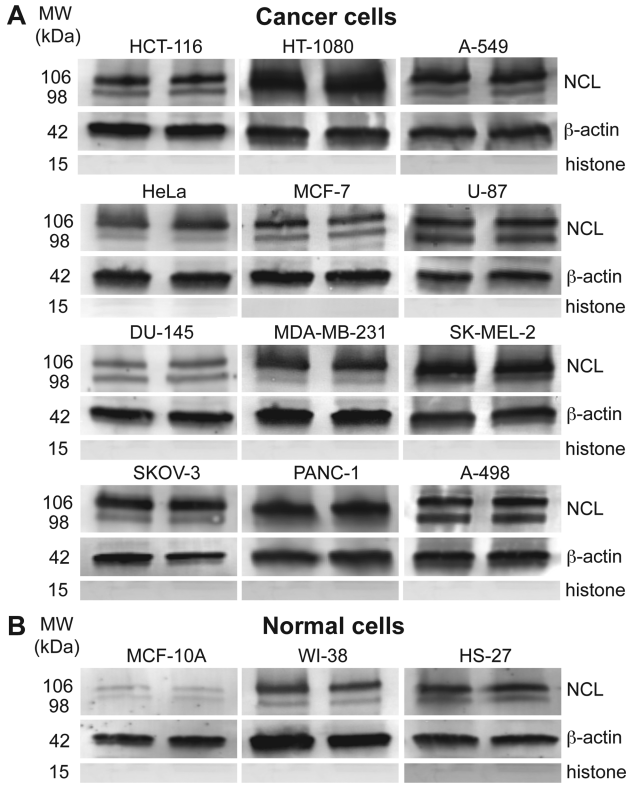

Figure 1. Nucleolin expression in non-nuclear extracts of cancer and normal cells. (A) Full-length (106 kDa) and the proteolysis product (98 kDa) of nucleolin appear in the non-nuclear lysates of all cancer cells. (B) MCF-10A cells show minimal expression of nucleolin, while fibroblast cells show nucleolin expression comparable to cancer cells.

gold precursor ($HAuCl_4$) in HEPES buffer, where HEPES acts as both a reducing agent as well as a shape-directing agent. The absence of surfactant in the AuNS synthesis is a major advantage over typical syntheses of gold particles, which require citrate ions or cetyl trimethylammonium bromide (CTAB) for stabilization; however, these molecules are toxic to healthy cells.[28−30] In addition, AuNS contains multiple branches (typically 2−9) that range in length from 10 to 65 nm (Figure 2A−B). The average hydrodynamic diameter measured by DLS was 39.2 ± 6 nm (Table S1). Because of this unique shape, extinction spectra of the nanoparticle suspension revealed that the localized surface plasmon resonance of AuNS was centered around 800 nm (Figure S1). This resonance can be tuned within the near-infrared (700−860 nm) region by controlling the size and shape of the gold nanostars by varying the concentration of HEPES buffer relative to $HAuCl_4$.[26,31] Important for potential *in vivo* work, the simplicity of synthesis, which only involves two reagents, can be easily scaled to 5 L (Figure 2C).

To synthesize the nanoconstructs, thiolated AS1411 was attached to the AuNS surface via gold−sulfur bonds in a 2-day "salt-aging" process (Supporting Information, Materials and Methods). The average hydrodynamic diameter of Apt-AuNS increased from 39.2 to 44.6 nm, and the surface charge decreased from −33.1 to −29.4 mV. Although we might have expected the surface charge to increase, the high concentrations of sodium ions surrounding the nanoconstructs tend to screen the negatively charged DNA.[32] Using a fluorescence calibration assay with Cy5-labeled AS1411 (Supporting Information, Materials and Methods), we determined that there were ca.

dx.doi.org/10.1021/mp4005657 | *Mol. Pharmaceutics* 2014, 11, 580−587

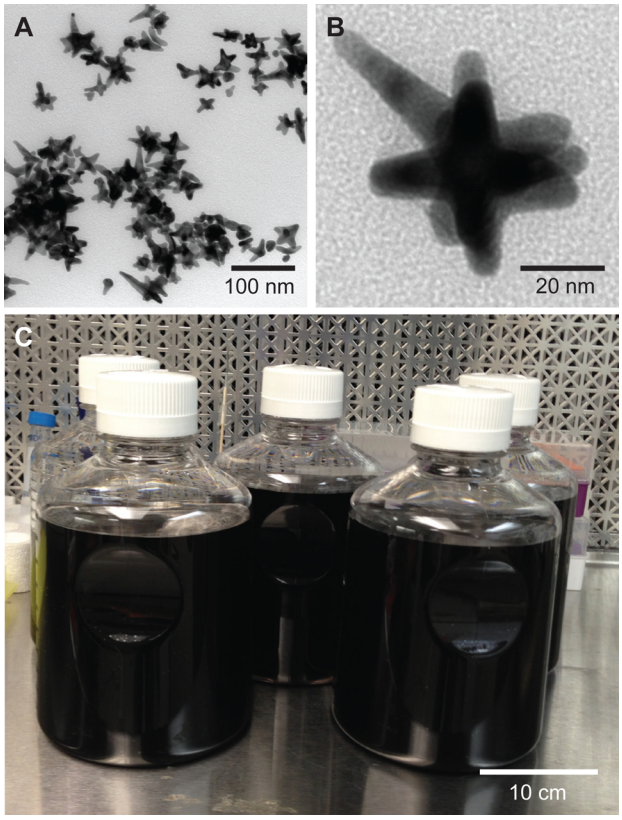

Figure 2. Gold nanostars (AuNS) as a drug delivery platform. (A) TEM image of multibranched AuNS. (B) Higher magnification TEM image of a representative AuNS shape, whose average hydrodynamic diameter is ca. 40 nm. (C) Scaled-up production of Apt-AuNS indicating that up to 5 L of Apt-AuNS can be synthesized in an hour.

110 strands of AS1411 on the surface of each AuNS. We found that Apt-AuNS was stable in aqueous solutions (e.g., DI water, PBS, HEPES buffer) at room temperature over two months (Figure S1).

Uptake of Apt-AuNS in Cancer and Normal Cells. Previous work revealed a 7 h incubation time with 0.3 nM Apt-AuNS was sufficient to deliver *in vitro* IC_{50} dosages of the nanoconstruct to HeLa cells.[26] Therefore, we used the same conditions to screen the 12-cancer cell line panel. To visualize uptake by confocal fluorescence microscopy, we labeled the 5′-end of Apt with Cy5 dye prior to attaching the aptamer to the AuNS (Cy5-Apt-AuNS). Figure 3A shows localization of the Cy5-Apt-AuNS (red fluorescence) in the cytoplasm and near the DAPI-stained nucleus (blue fluorescence) in all cancer cells. Also, surprisingly, we observed Cy5-Apt-AuNS signals in the cytoplasm of normal cells, especially the fibroblasts (Figure 3B). This uptake of Apt-AuNS in fibroblasts is consistent with a recent report that found high uptake of free AS1411 was possible in HS-27 via a different endocytosis mechanism from that in cancer cells.[33]

To quantify cellular internalization of Apt-AuNS in the panel, we measured the Au content using ICP-MS (Supporting Information, Materials and Methods). The highest level of Au content (24 ppt/cell) was found in PANC-1 (pancreatic cancer) cells, which was 12 times higher than that in normal MCF-10A (2 ppt/cell) (Figure 4). The Au content in fibroblasts (10 ppt/cell) was also much higher than that in MCF-10A cells (Figure 4). These quantitative results were in agreement with confocal microscopy images (Figure 3), where significantly higher Cy5 signals were observed in cancer cells and fibroblasts compared to MCF-10A cells. We expected that increased nucleolin expression would correlate with increased Au content across the cancer cell panel; however, no clear correlation between these two factors was observed. We hypothesize that cellular uptake can also depend on other factors, such as the doubling time of the cells, since cells tend to take up different amounts of particles at different stages of the cell cycle.[34] For example, HCT-116 cells have a much shorter doubling time (15 h) compared to HT-1080 cells (27 h). Thus, there is more time for HT-1080 cells to accumulate nanoconstructs, and uptake of Apt-AuNS was not directly proportional to nucleolin expression.

To determine whether there were differences in how Apt-AuNS were internalized by fibroblast cells and cancer cells, we used immunoblotting to compare the levels of nucleolin in the plasma membrane of normal and cancer cells. Although the non-nuclear nucleolin levels in the fibroblasts were comparable to that in cancer cells, plasma membrane extracts of HS-27 were much lower than those in HeLa and HT-1080 cells (Figure S2). Hence, the lack of nucleolin in plasma membranes of normal cells suggests that uptake is independent of surface-nucleolin and occurs through other endocytosis pathways, similar to previous reports.[33]

Decreased Bcl-2 mRNA Expression in Cancer Cells Incubated with Apt-AuNS. As described previously, AS1411 can bind to nucleolin and result in the downregulation of Bcl-2 in MCF-7 and MDA-MB-231 breast cancer cells.[20] Using quantitative real-time polymerase chain reaction (RT-PCR), we examined whether Apt-AuNS could also reduce Bcl-2 expression in other types of cancer cells by binding to nucleolin (Supporting Information, Materials and Methods). Compared to untreated cancer cells, the levels of Bcl-2 mRNA were reduced by at least two times in HT-1080 cells and up to four times in PANC-1 cells after incubation with Apt-AuNS (Figure 5). These decreases in gene expression are similar to that reported in breast cancer cells (MCF-7 and MDA-MB-231) after continuous treatment with 5 μM of free AS1411 for 72 h.[20] Importantly, the levels of Bcl-2 mRNA in all normal cells remained unchanged despite high Apt-AuNS uptake by the fibroblasts. Although Apt-AuNS can enter both normal and cancer cells, we expect the uptake to occur by different mechanisms based on previous reports of free AS1411.[33] We hypothesize that these differences can help explain why a reduction in Bcl-2 mRNA expression is observed in cancer cells but not in normal cells after treatment with Apt-AuNS (Figure 5). In effect, the nucleolin confined in and near the nucleus is not interacting with the nanoconstruct, and the levels of Bcl-2 will remain unchanged.

Because Bcl-2 mRNA functions as an antiapoptotic gene that prevents cancer cells from entering programmed cell death, downregulation of Bcl-2 expression can trigger apoptosis.[35] When cells undergo apoptosis, their caspase activities are often elevated.[36] We measured the caspase 3/7 activity of the 12-cancer cell panel (Supporting Information, Materials and Methods) and found that the caspase activities increased by ca. 1.5 times after a single 7 h incubation with Apt-AuNS. Note: we define the time after this 7 h incubation and after removal of the nanoconstructs as time t = 0. At t = 72 h, when control populations were close to 100% confluent, the activity of the proteases increased up to four times in HCT-116 (colon cancer) cells relative to untreated cells (Figure 6, blue bar). Cell viability was measured using a Cell-titer Blue assay to determine

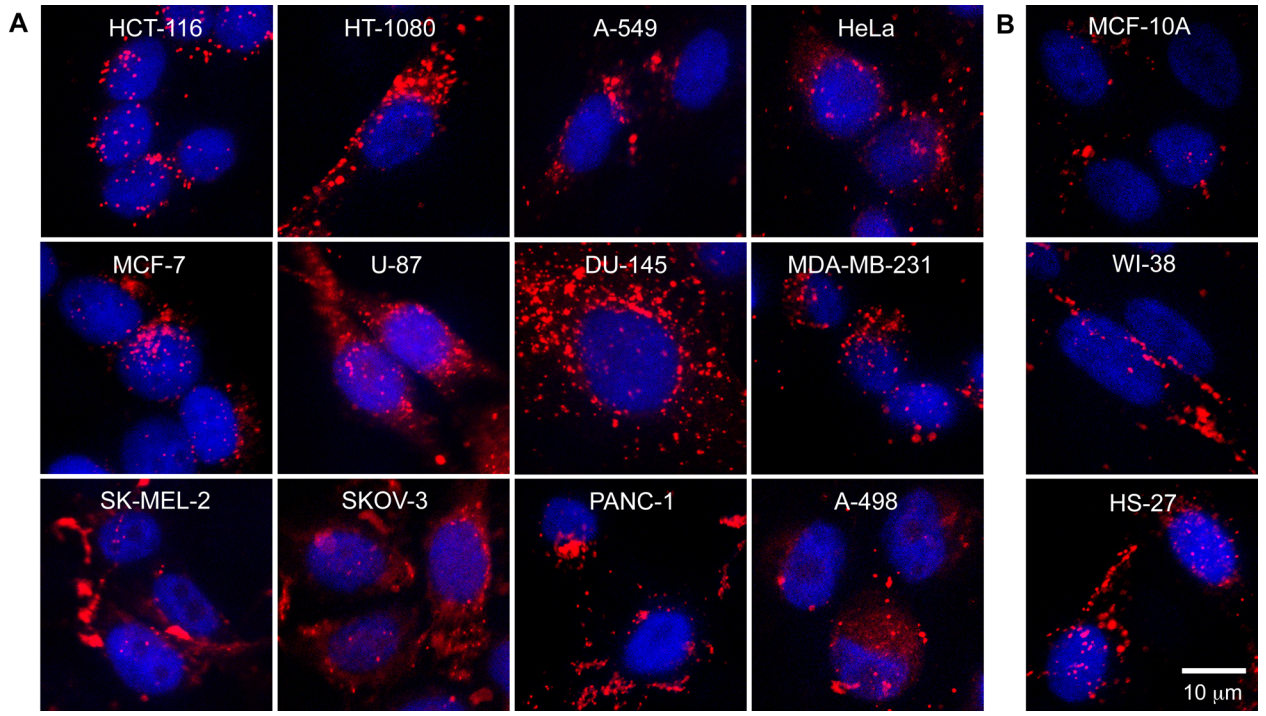

Figure 3. Uptake of Apt-AuNS in 12-cancer cell line panel and 3-normal cell line panel. Cy5-labeled Apt-AuNS (red) in the cytoplasm and near DAPI-stained nuclei (blue) in (A) cancer cells and (B) normal cells suggest that Apt-AuNS can be internalized. Cells are arranged in order of increased doubling time. All images were collected at the same magnification. Confocal images are 30 μm × 30 μm. Cancer cell panel: HCT-116 (colon), HT-1080 (connective tissue), A-549 (lung), HeLa (cervix), MCF-7 (breast), U-87 (brain), DU-145 (prostate), MDA-MB-231 (breast), SK-MEL-2 (skin), SKOV-3 (ovary), PANC-1 (pancreas), A-498 (kidney). Normal cell panel: MCF-10A (epithelial mammary), WI-38 (lung fibroblast), HS-27 (skin fibroblast).

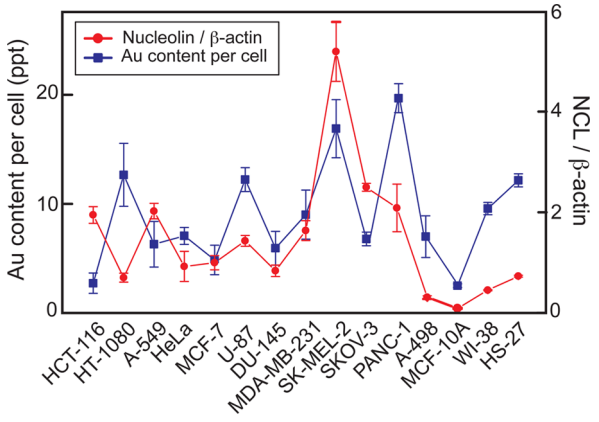

Figure 4. Apt-AuNS uptake and expression of nucleolin in plasma membrane and cytoplasmic in cancer and normal cells. Higher Au content and expression of non-nuclear nucleolin was found in cancer and fibroblast cell lines compared to mammary epithelial cells.

the percentage of live cells in the population (Supporting Information, Materials and Methods). Seventy-two hours after Apt-AuNS incubation, the average cell viability decreased by 25% (Figure 7, blue bar). The highest amount of cell death (ca. 40%) was recorded in SK-MEL-2 and DU-145 cells.

***In Vitro* Therapeutic Effects Generated by nM Concentration of Apt-AuNS.** Previously, we discovered that conjugating AS1411 onto AuNS carriers resulted in reduced dosages for efficacy in HeLa cells; low nM concentrations of Apt-AuNS[26] produced anticancer effects similar to μM of free AS1411.[16,37] We were interested in whether the *in vitro* efficacy of 0.3 nM Apt-AuNS (33 nM of Apt, ca. 110 strands per AuNS) in the 12-cancer cell lines would also be superior to free AS1411 at over 10 times the concentration. First, we observed an average reduction of 2 times of Bcl-2 mRNA expression in cancer cells treated with Apt-AuNS compared to those treated with free AS1411 (1.5 times) (Figure 5 and Table S1). These results suggest that Apt-AuNS can increase the destabilization of Bcl-2 mRNA and require less than a tenth of the aptamer dose.

In addition, the caspase 3/7 activity levels in cancer cells incubated with Apt-AuNS increased by 1.4 times compared to those with free AS1411 (Figure 6). Cell viability assays also indicated an average of 17% higher cancer cell death 72 h after incubation with Apt-AuNS than with free AS1411 (Figure 7 and Table S1). We attribute the superior biological effects of Apt-AuNS over free aptamer to two main factors: (1) Reformulation of AS1411 as Apt-AuNS. The nanoconstruct is more stable in physiological environments and the tight packing of Apt on the AuNS surface makes the aptamer less susceptible to degradation by serum or DNase compared to free Apt. Hence, the effects of Apt-AuNS could persist up to 72 h. (2) High local concentration of AS1411 uptake. Since each nanoconstruct can transport over 100 strands of AS1411 into cancer cells, high local concentrations of Apt can be internalized by cancer cells.

Light-Triggered Release of Apt from AuNS Increases Efficacy of *in Vitro* Treatment. Light-triggered release of Apt from AuNS near the cancer cell nucleus was found to increase *in vitro* therapeutic efficacy.[26] Our hypothesis is that this tandem treatment, where cancer cells are first incubated with Apt-AuNS and then exposed to fs pulses for 2 s (Apt-AuNS + *hν*) could also enhance *in vitro* efficacy compared to Apt-AuNS

dx.doi.org/10.1021/mp4005657 | *Mol. Pharmaceutics* 2014, 11, 580−587

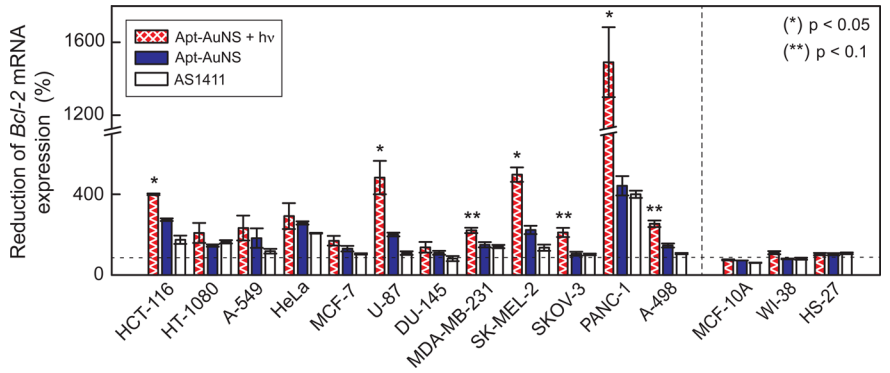

Figure 5. Downregulation of antiapoptotic Bcl-2 gene in cancer cells after treatment with Apt-AuNS. A 400% reduction of Bcl-2 mRNA expression was observed in PANC-1 cancer cells after treatment with 0.3 nM Apt-AuNS (33 nM AS1411) compared to untreated cancer cells. Gene expression was reduced further (200% to 1500%) in cancer cells after a single treatment with Apt-AuNS + *hν*. Only seven out of 12 cancer cells (HCT-116, HT-1080, HeLa, MDA-MB-231, PANC-1, SK-MEL-2, and U-87) treated with 450 nM free AS1411 decreased by minimal amounts. No change of Bcl-2 mRNA levels was found in normal cells. *p*-values were determined using a one-way ANOVA test. (*) and (**) indicate $p < 0.05$ and $p < 0.1$, respectively.

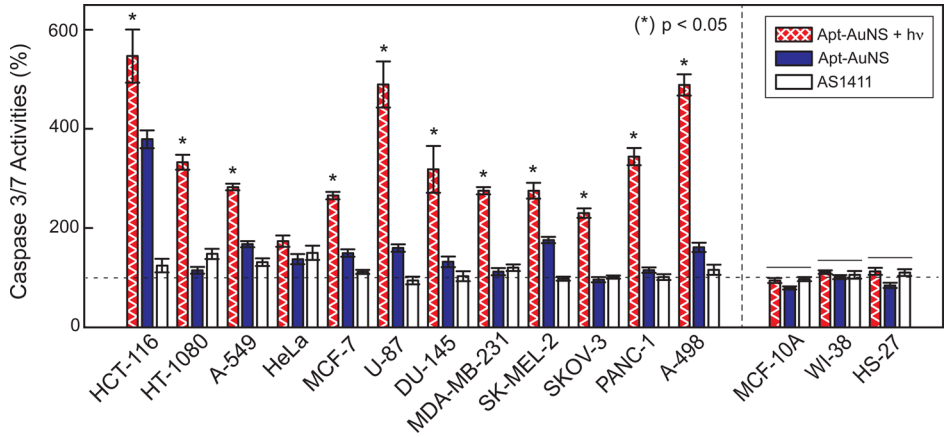

Figure 6. Elevation of caspase 3/7 activity in cancer cells after treatment with Apt-AuNS and Apt-AuNS + *hν*. Higher increases in caspase activities (up to 6-fold) are observed in all cancer cells treated with Apt-AuNS + *hν*. Up to a 4-fold increase of caspase 3/7 activities after treatment with Apt-AuNS indicates that large populations of cancer cells entered apoptosis. Negligible increase in caspase 3/7 activities in cancer cells from treatment with 450 nM AS1411 (less than 1.5-fold). Notably, there are no significant adverse effects observed in normal cells after exposure to laser irradiation. *p*-values were determined using one-way ANOVA test. Lines over bars indicate groups that are not significantly different.

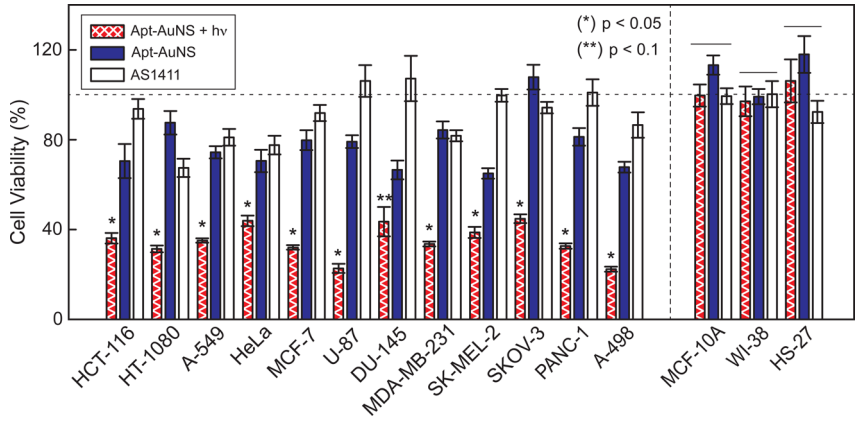

Figure 7. Light-triggered release of Apt from AuNS increases the percentage cell death. Cell viability analysis showed a 70% decrease of cell viability after aptamer release. Approximately 25% decrease in cell viability after treated with Apt-AuNS. Cancer cells treated with 450 nM of free AS1411 showed reduced effects on cell death (less than 10%) compared to those treated with 0.3 nM Apt-AuNS (33 nM AS1411) and three times lower than that from light-triggered treatment. No significant cell death was observed in any of the normal cell lines. *p*-values were determined using a one-way ANOVA test. Lines over bars indicate groups that are not significantly different. (*) and (**) indicate $p < 0.05$ and $p < 0.1$, respectively.

dx.doi.org/10.1021/mp4005657 | *Mol. Pharmaceutics* 2014, 11, 580−587

only in the cancer cell panel. First, we evaluated whether Apt-AuNS + $h\nu$ interfered with nucleolin-Bcl-2 mRNA interactions. We found an average of 3.6 times reduction of Bcl-2 mRNA expression, and this reduction was as high as 15 times in PANC-1 cells ($p < 0.05$) (Figure 5, hatched bar). The expression of Bcl-2 mRNA in cancer cells treated with Apt-AuNS + $h\nu$ was 1.6 times lower than that with only Apt-AuNS (Figure 5 and Table S1). These significant reductions in Bcl-2 mRNA expression suggest that intracellular release of high local concentration of Apt can further degrade the mRNA. The intracellular release of Apt also showed superior anticancer effects, where the average amount of cell death induced by Apt-AuNS + $h\nu$ increased by 55% compared to free AS1411 and 40% compared to Apt-AuNS only. The viability assay showed ca. 70% cell death in U-87, MCF-7, PANC-1 and A-498 (renal cancer) cells ($p < 0.05$) (Figure 7, hatched bars), which is comparable to the levels of cell death achieved in MCF-7 cells three days after a single dose of 10 μM free AS1411.[20] Furthermore, the caspase activities of all cancer cells treated with Apt-AuNS + $h\nu$ increased by an average of 3.4 times compared to 1.6 times with Apt-AuNS alone ($p < 0.1$) (Figure 6 and Table S1). This drastic increase of efficacy can be attributed to a highly localized concentration of Apt detached from nanocarriers by light-triggered release. Therefore, this tandem strategy can result in potent effects that require only minimal amounts of AS1411 (~33 nM) and that surpass results from μM concentrations of free AS1411.

■ CONCLUSIONS

In summary, we have reported a drug-loaded nanoconstruct—Apt-AuNS—that exhibits *in vitro* anticancer effects in a 12-cancer cell line panel with four major subcategories. We showed that the protein nucleolin is a viable surface target for Apt-AuNS by measuring expression in the plasma membrane and cytoplasm of the cancer cells. By binding to surface nucleolin, Apt-AuNS was taken up by 12 cancer lines. Importantly, the loading of AS1411 onto AuNS nanocarriers significantly improved the *in vitro* efficacy as a result of increased aptamer (drug) stability and presentation of high local concentrations of AS1411. Similar to free AS1411, Apt-AuNS resulted in downregulation of antiapoptotic Bcl-2 gene expression, elevation of apoptosis signals, and increased cell death in the panel. Light-triggered release further enhanced the *in vitro* efficacy by making available high local concentrations of Apt near the nucleus. Since Apt-AuNS shows anticancer effects on the 12-cancer cell line panel mediated by the ubiquitous protein nucleolin, we anticipate that this nanoconstruct can act as a platform for a new class of cell-type independent agents that could address some current challenges in targeted therapy.

■ EXPERIMENTAL SECTION

The full experimental details are provided in the Supporting Information. The most important information is summarized briefly below.

Cell Culture. All cultures were grown in a humidified incubator maintained at 37 °C with 95% air/5% CO_2. All cell lines were obtained from the American Type Culture Collection.

Synthesis of AuNS and Apt-AuNS. Gold nanostars (AuNS) were synthesized by reducing Au (III) chlorate in HEPES buffer to create biocompatible, surfactant-free gold nanoparticles for *in vitro* studies. The synthesis of Apt-AuNS was performed as previously reported.[24] The resonance wavelength of the AuNS and Apt-AuNS was measured using UV−vis spectroscopy. Particle size was determined using transmission electron microscopy (TEM) and dynamic light scattering (DLS).

Quantifying Number of AS1411 Strands on AuNS. Cy5-labeled aptamer 5′-(C6-S-S-C6)- Cy5-TTG GTG GTG GTG GTT GTG GTG GTG GTG G-3′ (Cy5-Apt) was used to estimate the number of aptamers on each particle. Attachment of Cy5-Apt to the AuNS followed the same procedure as described previously. Cy5-Apt-AuNS were treated with potassium cyanide (KCN) overnight to dissolve the Au core of the nanoconstruct and release Cy5 aptamer into the solution. The Cy5 fluorescence intensity of the KCN solution was measured using a NanoDrop spectrophotometer, and the concentration of AS1411 was determined based on the intensity of the Cy5 signal. This fluorescent assay indicated that approximately 110 strands of AS1411 were conjugated on a single AuNS.

Immunoblotting of Nucleolin. Cancer and normal cells were harvested from cell culture flasks. To determine expression of cytosolic nucleolin in cancer and normal cells, we lysed the cells on ice for 15 min in 5% NP40 lysis buffer (Invitrogen), followed by centrifugation at 10 000 *g* for 20 min. The supernatant contained the cytosolic extract, and the pellet contained the nuclear components. For plasma membrane extraction, cancer and normal cells were lysed in homogenized buffer (Abcam) and homogenized 50 times on ice using a Dounce homogenizer. Protein concentrations after the extractions were determined by the Bradford assay (Pierce). Aliquots of the cytosolic extracts containing 20 μg of protein were electrophoresed on a 10% Tris-HCl gel (Bio Rad) and transblotted using polyvinylidene fluoride (PVDF) membranes (Millipore). Antihuman nucleolin mAb (clone MS-3) (Santa Cruz Biotechnology, Inc.) and antimouse actin polyclonal antibody (Sigma-Aldrich) were used to label nucleolin and the housekeeping protein β-actin. The blot was stained with alkaline phosphatase-IgG secondary antibody. The bands were developed using enhanced chemifluorescence substrate (GE Healthcare) and visualized by Typhoon PhosphorImager (GE Healthcare). The amount of each protein in the blots was determined by counting the total number of pixels in each band (integrated density value). Values of nucleolin that were within the linear range of the assay were normalized to β-actin for the cytosolic extracts.

Confocal Imaging of Cy5-Labeled Nanoconstructs. Cells were incubated with 0.3 nM Cy5-labeled Apt-AuNS for 7 h and then washed three times with PBS. The cells were fixed with 4% paraformaldehyde (Sigma Aldrich). A drop of ProLong Gold Antifade reagent containing DAPI (Invitrogen) was used to mount each coverslip on a glass slide for confocal imaging. Confocal imaging was performed on an inverted Zeiss Axio Observer Z1 confocal microscope with a 40× objective and Zen acquisition software.

Quantification of Nanoconstruct Uptake in Cells. The cells were incubated with the nanoconstructs for 7 h at 37 °C in 5% CO_2 environment. After 7 h, excess Apt-AuNS were removed from the wells, and the cells were washed twice with ice cold PBS (Invitrogen). The cells were then harvested and suspended in 100 μL of phosphate-buffered saline (PBS). The cells were counted before being digested for 4 h at 75 °C in acid mixture containing 30% HCl (Sigma-Aldrich) and 70% HNO_3 (Sigma-Aldrich). After complete digestion of the AuNS,

dx.doi.org/10.1021/mp4005657 | *Mol. Pharmaceutics* 2014, 11, 580−587

the solution was diluted with Millipore water. The Au content was measured using ICP-MS.

Quantification of Bcl-2 mRNA Expression. Real-time polymerase chain reaction (qPCR) was used to quantify mRNA expression in cancer and normal cells. The assay was conducted using Power SYBR Green Cells-to-Ct Kit (Invitrogen). Cells were lysed using RNA lysis solution (Invitrogen). RNA lysates were reverse transcribed to synthesize cDNA. Primers for qPCR were designed using freely available software from IDT DNA. Identified primers were purchased from IDT DNA and tested for the amplification of a single uniform amplicon through analysis of SYBR melting curves for two cell lines (HeLa and A-549). All qPCR reactions were performed in 20 μL reaction mixtures. Each sample was run in triplicate with the IQ5 qPCR system (Bio-Rad). Each plate probed the expression of Bcl-2 and ACTB genes in the target cell lines. Real-time PCR data were analyzed using the comparative C_T method, also known as the $2^{-\Delta\Delta C_T}$ method, in which the expression of Bcl-2 mRNA was normalized to the expression of the housekeeping gene ACTB.

Biological Assays To Measure Caspase 3/7 Activity and Cell Viability. Apo-ONE Homogeneous Caspase-3/7 assay kit (Promega) and Cell-Titer Blue Cell viability assay (Promega) were used to measure caspase 3/7 activity and cell viability, respectively, in cancer and normal cells after treatment with Apt-AuNS, Apt-AuNS + $h\nu$, and 450 nM free AS1411.

■ ASSOCIATED CONTENT

Supporting Information

Experimental procedures and characterization of AuNS and Apt-AuNS; detailed procedures for immunoblotting, biological assays, and qPCR; immunoblotting of nucleolin expression in plasma membranes of cancer and normal cells; caspase activities and cell viability of cancer and normal cells after incubation. This material is available free of charge via the Internet at http://pubs.acs.org.

■ AUTHOR INFORMATION

Corresponding Author

*E-mail: todom@northwestern.edu.

Notes

The authors declare no competing financial interest.

■ ACKNOWLEDGMENTS

This work was supported by National Institutes of Health (NIH) Director's Pioneer Award DP1OD003899 and the H Foundation Cancer Research Fund, the Malkin Scholar Award, and the Rosenberg Award by the Robert H. Lurie Comprehensive Cancer Center at Northwestern University. We acknowledge Government support under FA9550-11-C-0028 and awarded by the Department of Defense, Air Force Office of Scientific Research, National Defense Science and Engineering Graduate (NDSEG) Fellowship, 32 CFR 168a (K.S.B.C.). Confocal imaging and metal analysis were performed at the Northwestern University Quantitative Bioelemental Imaging Center supported by National Science Foundation CHE-9810378/005 and NASA Ames Research Center NNA06CB93G. Biological assays were carried out in the High Throughput Analysis Laboratory, and UV−vis spectroscopic measurements and immunoblotting were performed at the NU Keck Biophysics Facility supported by Cancer Center Support Grant (NCI CA060553). TEM experiments were conducted at the Biological Imaging Facility. The authors are also thank the staff in the Developmental Therapeutic Core for assistance.

■ REFERENCES

(1) Harris, M. Monoclonal antibodies as therapeutic agents for cancer. *Lancet Oncol.* **2004**, *5*, 292−302.
(2) Brown, K. C. New approaches for cell-specific targeting: identification of cell-selective peptides from combinatorial libraries. *Curr. Opin. Chem. Biol.* **2000**, *4*, 16−21.
(3) Nahta, R.; Hung, M. C.; Esteva, F. J. The HER-2-targeting antibodies trastuzumab and pertuzumab synergistically inhibit the survival of breast cancer cells. *Cancer Res.* **2004**, *64*, 2343−2346.
(4) Ellis, L. M.; Hicklin, D. J. VEGF-targeted therapy: mechanisms of anti-tumour activity. *Nat. Rev. Cancer* **2008**, *8*, 579−91.
(5) Sawyers, C. Targeted cancer therapy. *Nature* **2004**, *432*, 294−7.
(6) Dexter, D. L.; Leith, J. T. Tumor heterogeneity and drug resistance. *J. Clin. Oncol.* **1986**, *4*, 244−57.
(7) Shipitsin, M.; Campbell, L. L.; Argani, P.; Weremowicz, S.; Bloushtain-Qimron, N.; Yao, J.; Nikolskaya, T.; Serebryiskaya, T.; Beroukhim, R.; Hu, M.; Halushka, M. K.; Sukumar, S.; Parker, L. M.; Anderson, K. S.; Harris, L. N.; Garber, J. E.; Richardson, A. L.; Schnitt, S. J.; Nikolsky, Y.; Gelman, R. S.; Polyak, K. Molecular definition of breast tumor heterogeneity. *Cancer Cell* **2007**, *11*, 259−73.
(8) Smith, I.; Procter, M.; Gelber, R. D.; Guillaume, S.; Feyereislova, A.; Dowsett, M.; Goldhirsch, A.; Untch, M.; Mariani, G.; Baselga, J.; Kaufmann, M.; Cameron, D.; Bell, R.; Bergh, J.; Coleman, R.; Wardley, A.; Harbeck, N.; Lopez, R. I.; Mallmann, P.; Gelmon, K.; Wilcken, N.; Wist, E.; Sanchez Rovira, P.; Piccart-Gebhart, M. J. 2-year follow-up of trastuzumab after adjuvant chemotherapy in HER2-positive breast cancer: a randomised controlled trial. *Lancet* **2007**, *369*, 29−36.
(9) Siegel, R.; DeSantis, C.; Virgo, K.; Stein, K.; Mariotto, A.; Smith, T.; Cooper, D.; Gansler, T.; Lerro, C.; Fedewa, S.; Lin, C.; Leach, C.; Cannady, R. S.; Cho, H.; Scoppa, S.; Hachey, M.; Kirch, R.; Jemal, A.; Ward, E. Cancer treatment and survivorship statistics, 2012. *CA Cancer J. Clin.* **2012**, *62*, 220−41.
(10) Bates, P. J.; Laber, D. A.; Miller, D. M.; Thomas, S. D.; Trent, J. O. Discovery and development of the G-rich oligonucleotide AS1411 as a novel treatment for cancer. *Exp. Mol. Pathol.* **2009**, *86*, 151−164.
(11) Borer, R. A.; Lehner, C. F.; Eppenberger, H. M.; Nigg, E. A. Major Nucleolar Proteins Shuttle between Nucleus and Cytoplasm. *Cell* **1989**, *56*, 379−390.
(12) Ginisty, H.; Sicard, H.; Roger, B.; Bouvet, P. Structure and functions of nucleolin. *J. Cell Sci.* **1999**, *112*, 761−772.
(13) Hovanessian, A. G.; Soundaramourty, C.; El Khoury, D.; Nondier, I.; Svab, J.; Krust, B. Surface Expressed Nucleolin Is Constantly Induced in Tumor Cells to Mediate Calcium-Dependent Ligand Internalization. *PloS One* **2010**, *5*, e15787.
(14) Soundararajan, S.; Wang, L.; Sridharan, V.; Chen, W. W.; Courtenay-Luck, N.; Jones, D.; Spicer, E. K.; Fernandes, D. J. Plasma Membrane Nucleolin Is a Receptor for the Anticancer Aptamer AS1411 in MV4−11 Leukemia Cells. *Mol. Pharmacol.* **2009**, *76*, 984−991.
(15) Keefe, A. D.; Pai, S.; Ellington, A. Aptamers as therapeutics. *Nat. Rev. Drug Discovery* **2010**, *9*, 537−550.
(16) Ireson, C. R.; Kelland, L. R. Discovery and development of anticancer aptamers. *Mol. Cancer Ther.* **2006**, *5*, 2957−62.
(17) Nimjee, S. M.; Rusconi, C. P.; Sullenger, B. A. Aptamers: An emerging class of therapeutics. *Annu. Rev. Med.* **2005**, *56*, 555.
(18) Otake, Y.; Soundararajan, S.; Sengupta, T. K.; Kio, E. A.; Smith, J. C.; Pineda-Roman, M.; Stuart, R. K.; Spicer, E. K.; Fernandes, D. J. Overexpression of nucleolin in chronic lymphocytic leukemia cells induces stabilization of bcl2 mRNA. *Blood* **2007**, *109*, 3069−3075.
(19) Sengupta, T. K.; Bandyopadhyay, S.; Fernandes, D. J.; Spicer, E. K. Identification of nucleolin as an AU-rich element binding protein involved in bcl-2 mRNA stabilization. *J. Biol. Chem.* **2004**, *279*, 10855−10863.

(20) Soundararajan, S.; Chen, W. W.; Spicer, E. K.; Courtenay-Luck, N.; Fernandes, D. J. The nucleolin targeting aptamer AS1411 destabilizes bcl-2 messenger RNA in human breast cancer cells. *Cancer Res.* **2008**, *68*, 2358−2365.
(21) Stuart, R. K.; Stockerl-Goldstein, K.; Cooper, M.; Devetten, M.; Herzig, R.; Medeiros, B.; Schiller, G.; Wei, A.; Acton, G.; Rizzieri, D. Randomized phase II trial of the nucleolin targeting aptamer AS1411 combined with high-dose cytarabine in relapsed/refractory acute myeloid leukemia (AML). *J. Clin. Oncol.* **2009**, *27*, 7019.
(22) Miller, D. M.; Laber, D. A.; Bates, P. J.; Trent, J. O.; Taft, B. S.; Kloecker, G. H. Extended phase I study of AS1411 in renal and non-small cell lung cancers. *Ann. Oncol.* **2006**, *17*, 147−148.
(23) Kim, B. Y.; Rutka, J. T.; Chan, W. C. Nanomedicine. *N. Engl. J. Med.* **2010**, *363*, 2434−43.
(24) Peer, D.; Karp, J. M.; Hong, S.; FarokHzad, O. C.; Margalit, R.; Langer, R. Nanocarriers as an emerging platform for cancer therapy. *Nat. Nanotechnol.* **2007**, *2*, 751−760.
(25) Girvan, A. C.; Teng, Y.; Casson, L. K.; Thomas, S. D.; Juliger, S.; Ball, M. W.; Klein, J. B.; Pierce, W. M., Jr.; Barve, S. S.; Bates, P. J. AGRO100 inhibits activation of nuclear factor-kappaB (NF-kappaB) by forming a complex with NF-kappaB essential modulator (NEMO) and nucleolin. *Mol. Cancer Ther.* **2006**, *5*, 1790−9.
(26) Dam, D. H.; Lee, J. H.; Sisco, P. N.; Co, D. T.; Zhang, M.; Wasielewski, M. R.; Odom, T. W. Direct observation of nanoparticle-cancer cell nucleus interactions. *ACS Nano* **2012**, *6*, 3318−26.
(27) Seferos, D. S.; Prigodich, A. E.; Giljohann, D. A.; Patel, P. C.; Mirkin, C. A. Polyvalent DNA nanoparticle conjugates stabilize nucleic acids. *Nano Lett.* **2009**, *9*, 308−11.
(28) Busbee, B. D.; Obare, S. O.; Murphy, C. J. An improved synthesis of high-aspect-ratio gold nanorods. *Adv. Mater.* **2003**, *15*, 414.
(29) Murphy, C. J.; Gole, A. M.; Stone, J. W.; Sisco, P. N.; Alkilany, A. M.; Goldsmith, E. C.; Baxter, S. C. Gold nanoparticles in biology: beyond toxicity to cellular imaging. *Acc. Chem. Res.* **2008**, *41*, 1721−30.
(30) Jana, N. R.; Gearheart, L.; Murphy, C. J. Seeding growth for size control of 5−40 nm diameter gold nanoparticles. *Langmuir* **2001**, *17*, 6782−6786.
(31) Xie, J. P.; Lee, J. Y.; Wang, D. I. C. Seedless, surfactantless, high-yield synthesis of branched gold nanocrystals in HEPES buffer solution. *Chem. Mater.* **2007**, *19*, 2823−2830.
(32) Massich, M. D.; Giljohann, D. A.; Schmucker, A. L.; Patel, P. C.; Mirkin, C. A. Cellular response of polyvalent oligonucleotide-gold nanoparticle conjugates. *ACS nano* **2010**, *4*, 5641−6.
(33) Reyes-Reyes, E. M.; Teng, Y.; Bates, P. J. A New Paradigm for Aptamer Therapeutic AS1411 Action: Uptake by Macropinocytosis and Its Stimulation by a Nucleolin-Dependent Mechanism. *Cancer Res.* **2010**, *70*, 8617−8629.
(34) Kim, J. A.; Aberg, C.; Salvati, A.; Dawson, K. A. Role of cell cycle on the cellular uptake and dilution of nanoparticles in a cell population. *Nat Nanotechnol.* **2012**, *7*, 62−8.
(35) Lam, M.; Dubyak, G.; Chen, L.; Nunez, G.; Miesfeld, R. L.; Distelhorst, C. W. Evidence That Bcl-2 Represses Apoptosis by Regulating Endoplasmic Reticulum-Associated Ca2+ Fluxes. *Proc. Natl. Acad. Sci. U.S.A.* **1994**, *91*, 6569−6573.
(36) Schwartz, G. K.; Shah, M. A. Targeting the cell cycle: a new approach to cancer therapy. *J. Clin. Oncol.* **2005**, *23*, 9408−21.
(37) Dapic, V.; Bates, P. J.; Trent, J. O.; Rodger, A.; Thomas, S. D.; Miller, D. M. Antiproliferative activity of G-quartet-forming oligonucleotides with backbone and sugar modifications. *Biochemistry* **2002**, *41*, 3676−3685.